RSC Advances

ROYAL SOCIETY OF CHEMISTRY

www.rsc.org/advances

RSC Advances

RSCPublishing

ARTICLE

Direct transformation of metallic copper to copper nanostructures by simple alcohol thermal treatment and their photoactivity

Cite this: DOI: 10.1039/x0xx00000x

Received 00th January 2012,
Accepted 00th January 2012

DOI: 10.1039/x0xx00000x

www.rsc.org/

Liangbin Xiong[ab], Huaqing Xiao[a], Qingdong Zeng[a], Boyun Wang[a], Sheng Wen[c]*, Bihui Li[c], Yaoming Ding[a] , and Huaqing Yu[a]*

A novel technique based on alcohol thermal treatment (ATT) was attempted to prepare copper nanostructures in a large scale. ATT provided copper sheet with high energy, resulting in the reconstruction of atoms into different atomic configurations and direct transformation of metallic copper to copper nanostructures. Copper nanostructures including nanobelts, nanowires and nanoparticles can be fabricated by adjusting the time of ATT. The ultraviolet visible diffuse reflectance spectra show ATT substantially enhanced the visible light (VL) absorbance of Cu nanostructures and Cu nanowires array gave the most efficient light harvesting in all of the samples. Photoelectrochemical and antibacterial experiments was carried out to investigate the photoactivity of different copper nanostructures. The results show the nanostructured surfaces by ATT significantly improved the photoactivity of copper sheets, among which copper nanowires demonstrated the highest photoactivity in bactericidal and photovoltaic effects since they completely inactivated 5-log of *Escherichia coli* K-12 within 1.5 h and produced 35 mV photovoltage under visible irradiation. The order of photoactive bactericidal effects for different nanostructured surfaces was also determined as Cu nanowires > Cu nanobelts > Cu nanoparticles > untreated Cu sheet, which was in accordance with that of VL absorbance and photovoltaic effects.

1. Introduction

There is increasing interest in pursuit of metal nanostructures for a variety of applications including plasmonics, nanoelectronics, chemical sensors, and biotechnology [1-4]. Particularly, copper (Cu) nanostructures are being extensively explored due to low cost compared to silver and gold, as catalysts [5], heat transfer systems [6], antibacterial materials [7], sensors [8], and transparent conducting electrodes for solar cell and flexible electronic devices [9, 10]. Thus, the preparation of Cu nanostructures is highly desired not only for the further development of synthetic strategies, but also for the examination of their properties.

Various synthetic methodologies of Cu nanostructures developed to date include solution-phase synthesis, vapor-phase synthesis and template-based synthesis [11]. Hydrothermal [12, 13] and chemical reduction methods [10] are the dominant strategies in solution-phase synthesis by using hydrazine [14], glucose [15] and two-ligand system [16] as reducing agents for production of Cu nanostructures in a large scale. In most of these cases, a stabilizer or organic compounds were frequently used as the precursor surfactant and template for preventing aggregation and controlling size as well as morphology [17, 18]. However, the use of strongly bonded protective agents may cause surface deactivation of copper nanostructures due to the coverage of copper nanostructures by the surfactants [19]. Moreover, they can interfere with the properties of the nanostructures in specific applications. Vapor-phase synthesis is typically used in Cu nanostructures [20, 21], but it involves tedious treatment process including the Cu precursor vaporization by heating at high temperatures and then the vapor flow over a solid substrate or supported catalyst in a relatively cooler zone to be condensed in a controlled atmosphere [22]. The template method [23, 24] is probably the most widely used method for the preparation of Cu nanostructures. It is easy to perform, and the morphology and crystallinity of nanostructures are relatively easily adjustable. However, the method consists of several steps, which is generally applicable for the preparation of very small amount of nanostructures.

Solvothermal method was frequently used to produce Cu oxide and Cu complex [25], but the study on direct transformation of metallic copper to copper nanostructures is still of absence so far. In this work, we describe an effective protocol for controllable preparation of copper nanostructures in a large scale by simple alcohol thermal treatment (ATT). In the new alcohol thermal method, metallic Cu was immersed in absolute alcohol filled in an autoclave for some time. In this case, the ATT provided Cu sheet with high energy, leading to direct transformation of metallic Cu to Cu nanostructures. The photoactivity of the selected samples was also investigated by the measurement of bactericidal and photovoltaic effects. The simplified ATT can be operated by a novel and cost efficient route without any tedious procedures, complicated apparatus, or any organic compounds and surfactants, which may promote

more research interest in the preparation and properties of Cu nanostructures.

2. Experimental section

2.1 Preparation and characterization of Cu nanostructures

A clean copper sheet (1 cm × 5 cm) was immersed in 80 ml of absolute alcohol solution filled in an autoclave. The temperature was kept at 160 °C and the treated time was 0.5, 1, 1.5, 2, 4, 6 and 8 h. The phase purity of untreated Cu sheet (i.e. Cu sheet before ATT) and all treated Cu sheets (i.e. Cu sheet after ATT) was characterized by x-ray powder diffraction (XRD) using an x-ray diffractometer (Y-2000) with Cu Kα radiation (λ = 1.5418 Å). A scan efficiency of $0.1°•S^{-1}$ was applied to record the powder patterns in the range of $10° \leq 2\theta \leq 80°$. Scanning electron microscopy (SEM) images were obtained on a JEOL SM-6700F microscope operated at 5 kV. Transmission electron microscopy (TEM) and high-resolution transmission electron microscopy (HRTEM) were carried out with JEOL JEM-100CXII. The ultraviolet visible diffuse reflectance spectra (UV-vis DRS) were carried out on a PerkinElmer Lambda 35 UV-vis Spectrophotometer. The photoelectrochemical experiments were conducted in a three-electrode electrochemical system with the treated and untreated Cu sheets as the working electrodes under visible light (VL) irradiation by using a 300 W Xenon lamp (Beijing Perfect Light Co. Ltd., Beijing) with a UV cutoff filter (λ < 420 nm) as the light source. The VL intensity was measured by a light meter (LI-COR, USA) and adjusted at 120 mW cm^{-2}. The counter and reference electrodes were platinum wire and saturated calomel electrode respectively. The open circuit photovoltage for all working electrodes was measured in 1.0 mM air-saturated Na_2SO_4 electrolyte by using PARSTAT 2273 electrochemical station.

2.2 Bacterial inactivation by Cu nanostructures in dark and under VL irradiation

The untreated Cu sheet and Cu sheets treated for 2, 4 and 6 h were selected as catalysts for inactivation of *Escherichia coli* K-12 (*E. coli*) in dark and under VL irradiation. The irradiation condition was the same as that in photoelectrochemical experiments. The bacteria strain *E. coli* was received from the American Type Culture Collection and chosen for this study. One pure bacterial colony grown on the Nutrient agar plate was inoculated in 2.5% nutrient broth solution at 37 ºC with 200 rpm agitation for 16 h. The culture was then washed twice with sterilized 0.9% NaCl solution (saline) by centrifugation at 5000 rpm for 5 min using a Hermle Z323 centrifuge (Hermle Labortechnik, Germany). The bacterial cells and photocatalyst were suspended in saline and the cell density was finally adjusted to about 2×10^5 colony forming unit (cfu)/mL by dilution with appropriate volume of saline to conduct different antibacterial experiments. The reaction temperature was maintained at 25 °C. At different time intervals, aliquots of the sample were collected and serially diluted with saline. 0.1 mL of the diluted sample was then immediately spread on nutrient agar (Lancashire, UK) plates and incubated at 37 °C for 24 h to determine the number of viable cells (in cfu). Light controls (light alone without photocatalyst) and dark controls (photocatalyst alone without light) were also carried out for each set of experiment. All experimental controls and treatments were performed in triplicates.

3. Results and discussion

3.1 XRD results

Fig. 1a shows the XRD pattern of untreated Cu sheet. Three peaks at 2θ = 43.2°, 50.4° and 74.1° could be indexed to the (111), (200) and (220) planes of the Cu as unique crystalline phase [26]. The d values (interplanar spacing) of (111), (200) and (220) planes were 2.087, 1.807, and 1.278 nm, respectively (JCPDS card No.04-0836). The locations of all diffraction peaks for Cu sheet after ATT for 2, 4 and 6 h are the same as that of untreated Cu sheet (Fig. 1b), suggesting that the alcohol thermal process did not change the phase composition of Cu sheet. However, we can see the intensity of all of the diffraction peaks changed after ATT by comparing Fig. 1a with Fig. 1b. The XRD pattern of untreated Cu sheet showed its peaks with preferential orientation along (111) direction, indicating the untreated Cu sheet have a relatively high percentage of (111) facets. The diffraction intensity of (111) and (220) plane decreased together with an increase in diffraction intensity of (200) plane, indicating that alcohol thermal process led to the reconstruction of atoms into different atomic configurations. No other peaks suggesting impurities, or significant changes in the peak locations of the XRD spectra, were detected after the ATT, indicating that pure Cu with a relatively high percentage of (200) facets were obtained under current alcohol thermal conditions. XRD patterns of Cu sheet after ATT for 0.5, 1, 1.5 and 8 h were all similar to Fig. 1b (data not shown here), suggesting that similar reconstruction of atoms happened and the ATT was not involved in a chemical reaction. The absolute alcohol just played the role of media transporting energy to Cu sheets, not participating chemical reaction [27]. We observed no significant change in the XRD data and color (golden yellow) of all the Cu nanostructures after they exposed to ambient atmosphere for 8 months, suggesting a good stability for the obtained samples.

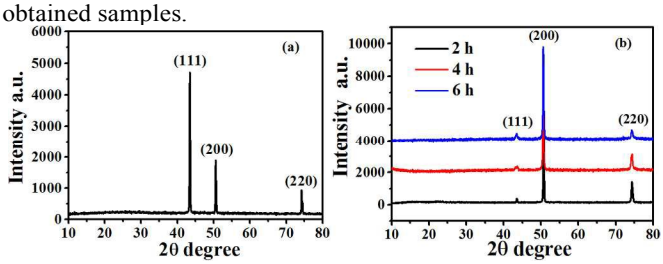

Fig. 1 XRD patterns of Cu sheet before (a) and after (b) ATT for 2, 4 and 6 h.

3.2 SEM results

Fig. 2 shows a representative panoramic view of the Cu sheet treated in absolute alcohol at 160 °C for different treated time. The untreated Cu sheet was composed of architectures with irregular shapes ranging from negligible nanostructures to primary microstructures (Fig. 2a). After ATT for 2 h, the architectures with irregular shapes were transformed to uniform nanowires with a diameter of 20-50 nm and a length of several micrometers (Fig. 2b). The bright field of TEM image for an individual nanowire reveals that the Cu nanowire grew well-defined in shape (Fig. 3a). Non-uniform contrast and disordered visible lattice fringes of HRTEM image (Fig. 3b) suggests the Cu nanowire was polycrystal due to small Cu nanocrystals assembling into the entire nanowire. The interplanar spacing of

the lattice fringes for a typical nanocrystal shown in the inset of Fig. 3b, corresponding to "B" region, is about 0.181 nm, which corresponds to the (200) plane of Cu nanowire (JCPDS card No.04-0836, 2θ=50.43°, d=1.807 nm), suggesting it grew along the [200] direction. After treated for 4 h in same condition, the uniform nanowires were changed into a scene of coexistence of nanowires and nanoparticles (Fig. 2c). Lastly, all nanowires were turned into nanoparticles (Fig. 2d) when the treated time up to 6 h.

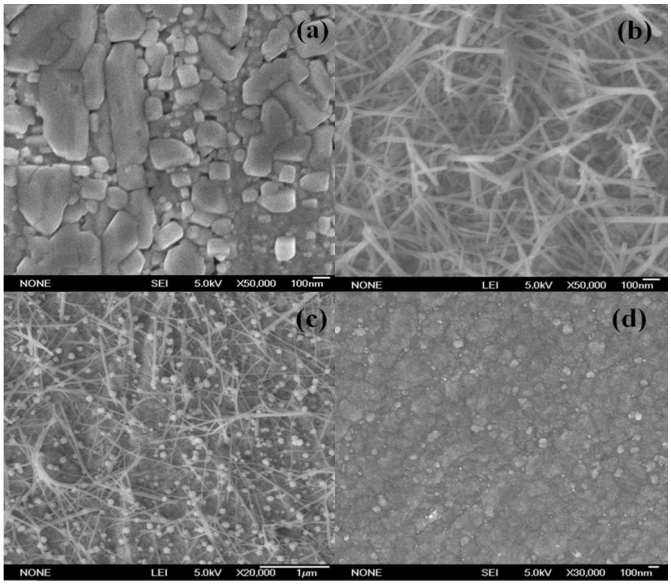

Fig. 2 SEM images of untreated Cu sheet (a) and treated Cu sheets in absolute alcohol filled in an autoclave at 160 °C for 2 (b), 4 (c) and 6 (d) h.

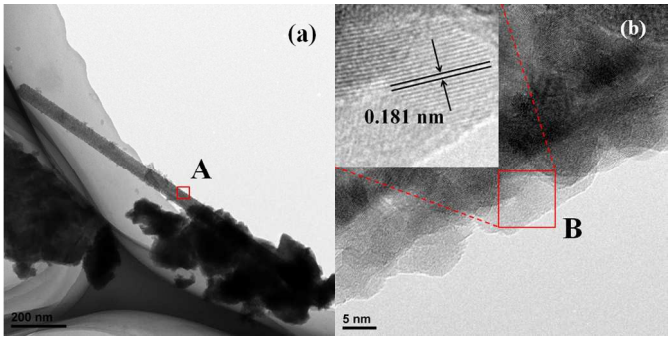

Fig. 3 TEM image (a) and HRTEM image corresponding to the red square "A" region (b) for Cu sheet treated in absolute alcohol for 2 h. Inset: the enlarged interplanar spacing of the lattice fringes corresponding to "B" region.

Comparing the SEM images of untreated Cu sheet and treated Cu sheets for different time (Figs. 2a~2d), we can imagine the most significant transformation of morphology occurred within the first 2 h, in which architectures with irregular shapes were totally changed into nanowires (Figs. 2a~2b). In order to explore the evolution of morphology within the first 2 h, we further carried out a new series of experiments with ATT time less than 2 h to record the information of morphology evolution. Figs. 3a~3a′ shows the morphology of Cu sheet treated for 0.5 h. Comparing Fig. 2a with Figs. 4a~4a′, we can observe that architectures with irregular shapes were transformed to something like polyhedrons with a uniform size of several hundred nanometers. The polyhedrons-like nanostructures then turned into nanobelts whose width decreased while length increased as ATT time increased (Figs. 4b~4b′ and 4c~4c′). When ATT time increased to 2 h, the nanobelts ultimately changed into nanowires (Fig. 2b).

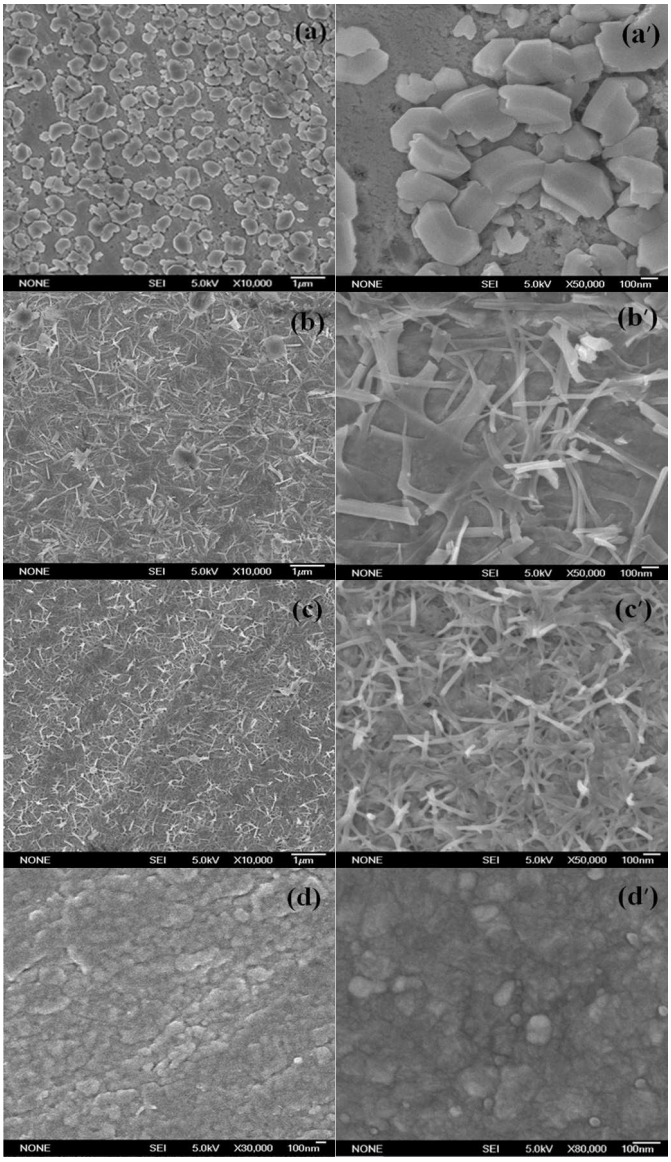

Fig. 4 SEM images of Cu sheets treated in absolute alcohol for 0.5 h (a), 1 h (b), 1.5 h (c) and 8 h (d) and their enlarged images (a′), (b′), (c′), and (d′), respectively.

3.3 Mechanism of morphology evolution

Based on the above experimental results and evolution scheme for the morphology of Cu sheets without ATT and with ATT for different time (Scheme 1), we proposed a possible mechanism for direct fabrication of copper nanostructures from metal copper with ATT. As mentioned in experimental section, Cu sheet was immersed in absolute alcohol solution filled in an autoclave. The high pressure and high temperature in the autoclave provided Cu sheet with high energy, rearranging the crystal grain of Cu sheet and leading to a tendency for Cu sheet transit to a higher surface energy. In this case, the particles with large size decreased to small ones in order to achieve a high surface free energy. Thus, as shown in Scheme 1.1,

architectures with negligible nanostructures and primary microstructures (Fig. 2a) turned to be polyhedrons with a uniform size of several hundred nanometers after Cu sheet was treated for 0.5 h (Figs. 4a~4a′). As a prolonged ATT time (from 0.5 h to 1 h), the treated Cu sheet gained more energy, leading to a gradual decrease of mass-surface ratio to achieve a higher total surface energy. Schemes 1.2~1.3 illustrate the process in which the polyhedrons turned into nanobelts (Figs. 4b~4b′) and then nanowires (Fig. 2b). As the continuous supply of energy, the mass-surface ratio of Cu sheet further decreased, some nanowires broke up into smaller pieces and coexistence of nanowires and nanoparticles appeared (Fig. 2c). Finally, as shown in scheme 1.4, all nanowires transformed to nanoparticles (Fig. 2d) after Cu sheet was treated for 6 h. Moreover, the morphology of Cu nanoparticles remained substantially unchanged even if the treated time was up to 8 h (comparing Fig. 2d with Figs. 4d~4d′), indicating that Cu nanoparticles crystals formed under current equilibrium conditions is determined by the relative order of surface energies [28]. In this case, Cu nanoparticles probably achieved a lowest mass-surface ratio and maximum total surface energy. In addition, as mentioned above, untreated Cu sheet has a relatively high percentage of (111) planes with d = 0.2087 nm while Cu sheet with ATT possesses dominant (200) planes with d = 0.181 nm. From the view of atomic arrangement of the Cu atoms, untreated Cu sheet with a wide d value has a tendency to transform into Cu sheet after ATT with a narrow one due to high pressure condition could give rise to the decrease of lattice parameters of Cu [29].

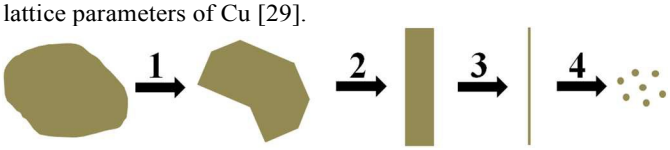

Scheme 1 Evolution scheme for the morphology of Cu sheets with ATT for different time.

3.4 UV-vis diffuse reflectance spectra

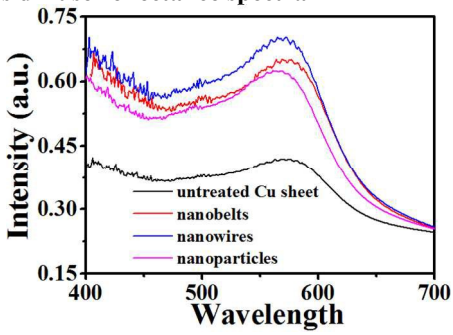

Fig. 5 UV-vis diffuse reflectance spectra of the untreated Cu sheet, Cu nanobelts, Cu nanowires and Cu nanoparticles.

Fig. 5 is the UV-vis DRS of the four samples. It is obvious that the VL absorption was substantially enhanced for Cu nanostructures and Cu nanowires array could absorb more VL than nanobelts, nanoparticles and untreated Cu sheet and Cu nanowires gave the most efficient light harvesting in the four samples. The curves in Fig. 5 are characteristic of broad absorption peaks around 570 nm, which attributed to the surface plasmon resonance (SPR) in the conduction bands of Cu nanostructures. As previously reported, the SPR range for Cu nanostructures was 550-590 nm because free electrons in the conduction band were induced and oscillated by light [30]. Compared with the untreated Cu sheet, slight blue shifts of the optical absorption were observed for the Cu nanostructures. All these variations of shifts in the SPR band of different Cu nanostructures can be ascribed to the difference in geometry which affects the scattering of light to diverse extent [31].

3.5 Photoelectrochemical properties

The photoactivity of the four samples was firstly investigated by photoelectrochemical measurements. Fig. 6 shows the curves of the photovoltage measured as a function of time for the treated copper sheet (Fig. 6a), Cu nanobelts (Fig. 6b), Cu nanowires (Fig. 6c), and Cu nanoparticles (Fig. 6d) electrodes under intermittent VL irradiation. Under the same intermittent irradiation, all treated Cu sheets electrodes resulted in photovoltage, but untreated Cu sheet had no significant response to the irradiation, suggesting that Cu nanostructures fabricated by ATT resulted in the photovoltage. It is well known that electrons in the conduction band of nanoscale metallic materials oscillate upon excitation from appropriate irradiation, leading to a phenomenon of SPR. This oscillation induces charge separation between the free electrons and the positive metal core [32]. The free electrons may transfer to the solution and leave behind the metal core with positive charge in the electrodes, resulting in positive photovoltage. The photovoltage produced in Cu nanowires electrode was about 35 mV photovoltage (Fig. 6c), much higher than that in Cu nanobelts (11 mV) and nanoparticles electrodes (5 mV). The better photovoltaic property of the Cu nanowires demonstrates that nanowires may have a better photo-generated charge separation than nanobelts and nanoparticles. Indeed, the aligned nanowires could absorb more VL than nanobelts and nanoparticles according to the data of UV-vis DRS. Also, the aligned nanowires can contact the electrolyte with a larger interface area than nanobelts and nanoparticles, which benefits to charge separation [33].

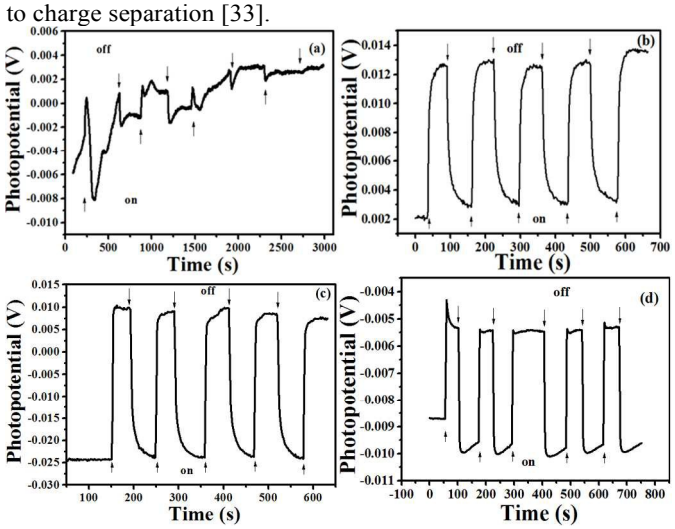

Fig. 6 Plots of open circuit photovoltage measured as the function of time with intermittent VL irradiation for untreated Cu sheet (a), Cu nanobelts (b), Cu nanowires (c) and Cu nanoparticle (d) electrodes, respectively.

3.6 Antibacterial activity

We further investigated the photoactivity of the four samples for the inactivation of *E. coli* in dark and under VL irradiation. Fig. 7 shows the inactivation kinetics of *E. coli* in different conditions. Light control showed the bacterial population remained essentially unchanged within 2 h, suggesting *E. coli* was not inactivated only under VL irradiation. In dark control,

the bacterial population reduced about 1 log for all of the selected samples, indicating they have a mild and similar toxicity to *E. coli*. The metallic Cu bactericide properties have been known for a long history [34] and its nanostructured counterparts were extensively studied due to its antibacterial activity [7, 35-37]. Under VL irradiation, the inactivation efficiency was substantially improved. About 5-log *E. coli* could completely be inactivated within 1.5 and 2 h for Cu nanowires and Cu nanobelts, respectively. As for Cu nanoparticles and untreated Cu sheet, about 4.5 and 3-log reduction of *E. coli* could be obtained within 2 h, respectively. The results indicate all of them had a photocatalytic inactivation activity towards *E. coli*. The results agree with that reported by A. Ehiasarian *et al*. [38] who demonstrated sputtered Cu film presented a good photoactivity for the inactivation of *E. coli*. Cu nanowires completely inactivated 5-log of *E. coli* within 1.5 h under VL irradiation, demonstrating the highest photoactivity in bactericidal in all samples. The order of photoactive bactericidal effects for all samples was also studied. It was determined as Cu nanowires > Cu nanobelts > Cu nanoparticles > untreated Cu sheet, which was in accordance with that of VL absorbance and photovoltaic effects. Photoactive bactericidal effects may originate from oxidative stress induced by reactive oxygen species (ROS) generation in nanostructured systems, which is thought to be the main mechanism of their antibacterial activity [39]. When irradiated by VL, electrons in the conduction band of Cu nanostructures oscillate due to SPR, leading to charge separation between the free electrons and the positive metal core [30]. The free electrons may transfer to the solution and react with molecular oxygen to produce $\bullet O^{2-}$, then H_2O_2 and •OH *et al*. through a reductive process. The positive metal core may abstract electrons from water and/or hydroxyl ions to generate •OH through an oxidative process. Consequently, these ROS ($\bullet O^{2-}$, H_2O_2, and •OH *et al*.) are considered to be the major reactive species contributing to the major oxidative stress in biological systems. Considering the order of photoactive bactericidal effects in accordance with that of VL absorbance and photovoltaic effects for all samples, we think it is probably that the more VL absorbed by a sample, the more electrons separated from the positive metal core, the higher photovoltaic effects appeared, and the more ROS produced, resulting in the higher bactericidal activity under VL irradiation. Further exploration of photoactive bactericidal mechanism is still under way.

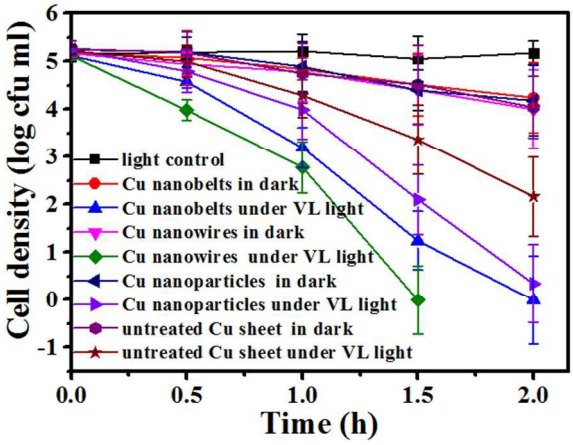

Fig. 7 Inactivation of *E. coli* by untreated Cu sheet and Cu nanobelts, nanowires and nanoparticles in dark and under light irradiation. Initial *E. coli* concentration, about 2×10^5 cfu mL^{-1}.

Conclusions

A new technique based on ATT has been developed to prepare Cu nanostructures in a large scale. Direct transformation of metallic Cu to Cu nanostructures can be achieved by immersing Cu sheet in absolute alcohol filled in an autoclave for some time. Cu nanostructures including nanobelts, nanowires and nanoparticles can be fabricated by adjusting the time of ATT. ATT significantly improved the VL absorbance and photoactivity of copper sheets. Copper nanowires can completely inactivate 5-log of *E. coli* within 1.5 h and produced 35 mV photovoltage under VL irradiation, demonstrating much higher photoactivity in bactericidal and photovoltaic effects than other samples. The order of VL absorbance, photoactive bactericidal and photovoltaic effects for all samples was the same and determined as Cu nanowires > Cu nanobelts > Cu nanoparticles > untreated Cu sheet.

Acknowledgements

This work was supported by China Postdoctoral Science Foundation (2015M572187), Hubei Provincial Department of Education (D20152702), the National Natural Science Foundation of China (Grant no. 61370223 and 51303048) and the Natural Science Foundation of Hubei Province (Grant no. 2014CFB579).

Notes and references

[a]*School of Physics and electronic-information Engineering, Hubei Engineering University, Xiaogan, 432000, China*.
E-Mail: yuhuaqing@126.com, Tel: +86-712-234-5441
[b]*Key Laboratory of Artificial Micro- and Nano-structures of Ministry of Education of China, School of Physics & Technology, Wuhan University, Wuhan, Hubei 430072, P. R. China.*
[c]*College of Chemistry and Materials Science, Hubei Engineering University, Xiaogan 432000, China*
E-Mail: shengwen_hber@163.com, Tel: +86-712-234-5464

1 S. Linic, U. Aslam, C. Boerigter and M. Morabito. *Nat. Mater.* 2015, **14**, 567-576.
2 T. F. REN and X. Ling *Chin. J. Cata.* 2000, **21**, 455-458.
3 F. Meng and S. Jin. *Nano Lett*. 2012, **12**, 234-239.
4 O. Y. Loh and H. D. Espinosa. *Nat. Nanotechnol*. 2012, **7**, 283-295.
5 Z. Chen, A. R. Rathmell, S. Ye, A. R. Wilson and B. J. Wiley. *Angew. Chem. Int. Ed. Engl*. 2013, **52**, 13708-13711.
6 J. A. Eastman, S. U. S. Choi, S. Li, W. Yu and L. J. Thompson. *Appl. Phys. Lett*. 2001, **78**, 718-720.
7 C. H. C. C. Kaweeteerawat, K. R. Roy, R. Liu, R. B. Li, D. Toso, H. Fischer, A. Ivask, Z. X. Ji, J. I. Zink, Z. H. Zhou, G. F. Chanfreau, D. Telesca, Y. Cohen, P. A. Holden, A. E. Nel, and H. A. Godwin. *ACS Nano* 2015, **9**, 7215-7225.
8 Y. Liu, Z. Liu, N. Lu, E. Preiss, S. Poyraz, M. J. Kim and X. Zhang. *Chem. Commun*. 2012, **48**, 2621-2623.
9 S. Ye, A. R. Rathmell, Z. Chen, I. E. Stewart and B. J. Wiley. *Adv Mater*. 2014, **26**, 6670-6687.
10 S. Ye, A. R. Rathmell, I. E. Stewart, Y. C. Ha, A. R. Wilson, Z. Chen and B. J. Wiley. *Chem Commun*. 2014, **50**, 2562-2564.

11 S. Bhanushali, P. Ghosh, A. Ganesh and W. Cheng. *Small* 2015, **11**, 1232-1252.
12 Y. Zhao, Y. Zhang, Y. Li and Z. Yan. *New J. Chem*. 2012, **36**, 130-138.
13 Y. X. Zhao, Y. Zhang, Y. P. Li, Z. Y. He and Z. F. Yan. *RSC Adv*. 2012, **2**, 11544-11551.
14 A. R. Rathmell, S. M. Bergin, Y. L. Hua, Z. Y. Li and B. J. Wiley. *Adv. Mater*. 2010, **22**, 3558-3563.
15 M. Jin, H. Zhang, J. Zeng, Z. Xie, and Y. Xia, *Angew. Chem. Int. Ed*. 2011, **50**, 10560-10564 .
16 D. Zhang, M. Wen, D. Weng, X. Cui, J. Sun, H. Li, and Y. Lu. *J. Am. Chem. Soc*. 2012, **134**, 14283-14286.
17 Y. Tan, X. Xue, Q. Peng, H. Zhao, T. Wang and Y. Li. *Nano Lett*. 2007, **7**, 3723-3728.
18 S. Deki, K. Akamatsu, T. Yano, M. Mizuhata and A. Kajinami. *J. Mater. Chem*. 1998, **8**, 1865-1868.
19 H. R. Ong, M. M. R. Khan, R. Ramli, Y. Du, S. Xi and R. M. Yunus. *RSC Adv*. 2015, **5**, 24544-24549.
20 S. N. Mohammad. *Nano Lett*. 2008 **8**, 1532-1538.
21 H. Choi and S. H. Park. *J. Am. Chem. Soc*. 2004, **126**, 6248-6249 .
22 W. A. Bryant. *J. Mater. Sci.* 1977, **12**, 1285-1306.
23 A. Mignani, B. Ballarin, E. Boanini and M. C. Cassani. *Electrochim Acta*. 2014, **115**, 537-545.
24 S. Shin, B. S. Kim, K. M. Kim, B. H. Kong, H. K. Cho and H. H. Cho. *J. Mater. Chem*. 2011, **21**, 17967-17971.
25 Z. Wang, F. B. Su, S. Madhavi and X. W. Lou. *Nanoscale* 2011, **3**, 1618-1623.
26 N. Yang, Z. Wang, L. Chen, Y. Wang and Y. B. Zhu. *Int. J. Refract. Met. Hard Mater*. 2010, **28**, 198-200.
27 L. Xiong, S. Huang, X. Yang, M. Qiu, Z. Chen and Y. Yu. *Electrochim. Acta*. 2011, **56**, 2735-2739.
28 M. J. Siegfried and K. S. Choi. *Adv Mater*. 2004, **16**, 1743-1746.
29 C. Q. Zheng, J. Lin, Y. Xie, S. J. Liu. *Journal of Beijing Normal University* 2007, **43**, 613-616.
30 Z. Yin, S. K. Song, D. J. You, Y. Ko, S. Cho, J. Yoo, S. Y. Park, Y. Piao, S. T. Chang and Y. S. Kim. *Small* 2015, **11**, 4576-4583.
31 R. Kaur and B. Pal. *Appl. Catal. A: General*. 2015, **491**, 28-36.
32 K. Thorkelsson, P. Bai and T. Xu. *Nano Today*. 2015, **10**, 48-66.
33 C. M. McShane and K. S. Choi. *J. Am. Chem. Soc*. 2009, **131**, 2561-2569.
34 M. D. F. Simon, W. J. Gould, A. F. Kelly, M. Morgan, J. Kenny, D. P. Naughton. *Annals Microbiol*. 2009, **59**, 151-156.
35 G. Grass, C. Rensing and M. Solioz. *Appl. Environ. Microbiol*. 2011, **77**, 1541-1547.
36 T. Y. Klein, J. Wehling, L. Treccani and K. Rezwan. *Environ. Sci Technol*. 2013, **47**, 1065-1072.
37 B. Jia, Y. Mei, L. Cheng, J. Zhou and L. Zhang. *ACS Appl. Mater. Interfaces*. 2012, **4**, 2897-2902.
38 A. Ehiasarian, C. Pulgarin and J. Kiwi. *Environ. Sci. Pollut. Res. Int*. 2012, **19**, 3791-3797.
39 Y. Li, W. Zhang, J. Niu and Y. Chen. *ACS Nano* 2012, **6**, 5164-5173.

Graphical Abstract

Direct transformation of metallic copper to copper nanostructures by simple alcohol thermal treatment and their photoactivity

Liangbin Xiong[ab], Huaqing Xiao[a], Qingdong Zeng[a], Boyun Wang[a], Sheng Wen[c]*, Bihui Li[c], Yaoming Ding[a] , and Huaqing Yu[a]*

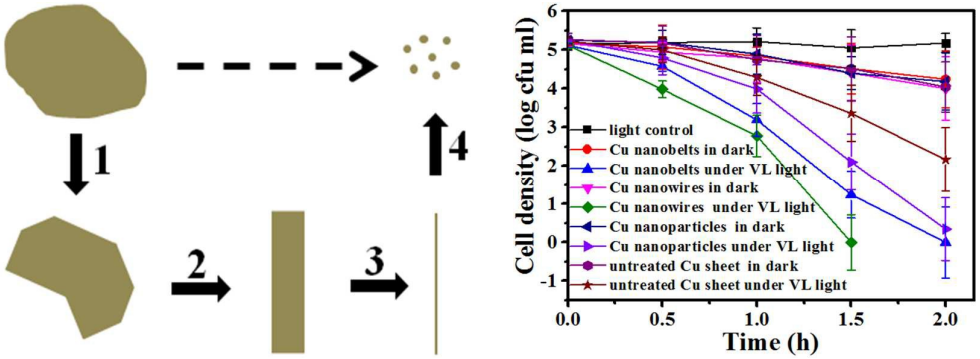

Evolution scheme for the morphology of Cu sheets with ATT for different time (left). Inactivation of *E. coli* by untreated Cu sheet and Cu nanobelts, nanowires and nanoparticles in dark and under light irradiation (right).